

Article

On the Stability of the Melt Jet Stream during Casting of Metallic Glass Wires

Ayo Olofinjana ^{1,*} and Nyuk Yoong Voo ²

¹ School of Science and Engineering, University of the Sunshine Coast, Maroochydore DC, QLD 4558, Australia

² Faculty of Science, Universiti Brunei Darussalam, Jalan Tungku Link, BE1410, Brunei Darussalam; E-Mail: nyukyoong.voo@ubd.edu.bn

* Author to whom correspondence should be addressed; E-Mail: aolofinj@usc.edu.au; Tel.: +61-7-5456-5987; Fax: +61-7-5456-5453.

Academic Editors: K. C. Chan and Jordi Sort Viñas

Received: 19 May 2015 / Accepted: 2 June 2015 / Published: 8 June 2015

Abstract: The factors that affect the stability of the melt stream during the casting of wire directly from the melt have been investigated. It is shown that the criticality of process parameters centres mostly on the forces imposed on the melt stream at confluence with the cooling water. The analysis of these forces indicated that the shear component of the disturbance is dependent on the ratio of the velocity of the melt stream (v_m) to that of the cooling water (v_w) in accord with results obtained from previous experiments. The role of oxide-forming elements in widening the process parameters range is attributed to the increased stability of the melt stream due to the additional shear force resistance offered by the solid oxide layer. The roles of Cr and Si oxides in stabilising the melt stream are confirmed by X-ray photoelectron spectroscopy (XPS) of wire indicating the presence of these oxides on fresh as-cast wires. Melt superheat and nozzle clearance distance are not strictly stream stability factors, but rather their role in glass formation prescribes optimal limits for fully amorphous wire.

Keywords: metallic glass; amorphous alloy; wire casting; multi-strand casting; jet stability

1. Introduction

The ability to cast wire directly from melt provides such an obvious production process advantage that it has long attracted attention. One of the earliest methods proposed dates back to 1882 [1] and, more recently, many more processes have been proposed [2–9] to achieve this. Since molten metal unlike oxide melts are known to have very low viscosities, the success of the proposed methods relies heavily on maintaining continuous flow of mass on the transition from liquid to solid without stream breaking. Many of the early attempts, however, were fraught with difficulties in maintaining a stable melt jet at the interaction of the melt stream and the static quenching medium which inevitably has an impact due to the velocity resistance when the jet comes into contact with the quenching medium. Recent reports on the production of round sectioned wire from melt are therefore restricted to a few more modern processes [10–14] utilising a dynamic quenching medium. In these, the non-static nature of the quenching medium reduced the momentum difference and, thus, significantly reduced the impact on the stream and, to a large extent, determined the flow and shape of the final product.

Though the early attempts were not aimed at rapid solidification, the task of forming wires of small diameters directly from melt, apart from providing a technological shortcut in production route, also implies the inherent rapid solidification of the melt which could lead to the vitrification of a readily glass-forming alloy. The range of wire castable alloys [7,10] are mostly (except for a few) readily glass forming alloys. Magnetic Fe- and Co-based amorphous alloys are now routinely cast in diameters in the order of 100 μm . The potential applications of amorphous wire in magnetic devices are now well known [13–19] and improvements in production techniques are being pursued. Presently, only the Taylor-Ulitovsky and the rotating water bath processes are consistently used [14,20] to make directly cast amorphous wires for magnetic applications. The versatility of Taylor–Ulitovsky method is demonstrated in the wide range of compositions [11,21–24] from which metallic glass microwires can be produced, including Heusler-type alloys [25–29] that are being proposed for magnetic shape memory alloys (MSMA) owing to their giant magnetic field induced strain.

These new interests in magnetic applications (such as microwires for giant magneto impedance [30]) have led to continually increased interest in improving methods for casting metallic glass wires. A recent review [22] of metallic glass microwires as a multifunctional composite suggest melt extraction and the Taylor–Ulitovsky methods as the techniques of choice for making suitable microwires. In the Taylor–Ulitovsky process, the use of a glass coating removed the inherent problem of melt stream stability and, in principle, could be used for any alloy for which a matching glass could be found. It remains the method of choice for casting metallic glass microwires with diameters typically less than 60 μm . It is however limited in its applicability, especially regarding the production of metallic glass wires with larger diameters. To allow the imposition of an amorphous structure in the Taylor–Ulitovsky methods, critical cooling rates imposed by thermo-kinetic factors required the diameters of the cast wires to be less than 60 μm , translating to cooling rates greater than 10^5 K s^{-1} . The chemical removal of the glass coating by hydrofluoric acid (HF) dissolution [30–32] is a necessary part of this process and can further complicate the development. Nonetheless, it has successfully been used [9,13,16,21–24,28,33,34] to prepare high quality metallic glass wires with diameters less than 60 μm . However, for larger diameter glassy wire, direct containerless solidification of the melt stream is required.

The rotating water bath process, however, has been used to produce wires of approximately 100 μm diameter in a variety of compositions [6,10,13]. The cooling rates for the diameter achieved is of the order of $10^5\text{--}10^6 \text{ K s}^{-1}$, and is enough to vitrify most readily glass-forming alloys. We have explored the development of direct casting in a multi-stream mode [35,36] where it was demonstrated that the productivity of wire production could be increased through multi-streaming without adversely affecting the wire forming and vitrification processes. This process has potential for scale up, but inconsistency in products after several attempts required the clarification of the many varied factors that affect the melt stream stability and, consequently, the quality of the cast metallic glass wires. It represents the only method by which larger diameters of up to 150 μm glassy wires can be produced directly from melt. The main problem is to understand factors that affect the stability of melt jet stream in order to consistently produce high quality metallic glass wires. Here, discussion is focussed on how the critical process parameters might have affected the stability of the melt streams. It is hoped that an understanding of such problems would contribute to new developments in the process and alloy selection for multi-stream casting of metallic glass wires directly from melt. Such relatively thick metallic glass wires are known for their magnetic bi-stability and very high strength. It is expected that a high volume production would promote their use as structural reinforcement and possible magnetic applications.

2. Experimental Section

2.1. Wire Casting

Thirty-five grams ingots of $\text{Fe}_{100-x-y}\text{Cr}_x\text{Si}_y\text{B}_{15}$ alloys were produced by melting the pure constituent elements in a boron nitride crucible in an induction furnace. Each ingot was re-melted in a quartz crucible in the base of which were laser drilled nozzles as described previously [35]. Single and multi-orifice nozzles were used to study the fluid flow in order to establish the flow coefficients determined by the specific crucible nozzle geometry. The temperature of the melt was monitored via a boron nitride shielded Pt/PtRh (13%) thermocouple. The mV signal from the thermocouple was connected via a modified IC to the electronic control module of the rf generator, such that it was possible to program the generator through the thermocouple feedback. In all cases, the melt temperature could be maintained within $\pm 10 \text{ K}$ of specified temperature.

The flow of liquid metal through the nozzles was initiated by applying an argon gas pressure above the melt surface in the quartz crucible. The gas pressure was monitored and controlled by a pressure transducer. The rotating speed of the bath was monitored by an optical tachometer. The melt streams were projected into the rotating water bath. The success of filament cast depended on the stability of the melt stream which was affected by a number of factors which are discussed herein.

2.2. Determining Melt Stream Velocity

The accurate determination of the jet velocity is an important factor in optimising other process variables for successful wire casting. The effects of gravity and surface tension have opposing effects on the magnitude of the final velocity of the melt stream, and in any case, their combined effect is negligible compared to the applied pressure head. The stream velocity v_m as a result of gas pressure P was calculated from a modified Bernoulli equation [37]:

$$v_m = C_f \left(\frac{2P}{\rho} \right)^{1/2} \quad (1)$$

where ρ is the density of melt and C_f is a flow coefficient determined from flow curves by plotting the square of the flow rate against nozzle diameters in water experiments. Water was used as the experimental liquid to avoid the effects of high temperatures on thermal distortion of the geometrical factor that is being corrected for. Typical flow curves using single orifice laser drilled nozzles are shown in Figure 1. The linearity of the curves validated the use of flow coefficient C_f to determine the final velocity according to Equation (1). The derived relationship was used to calibrate the velocity of jets for a given pressure and was found to be adequate in the pressure range of 0.3–0.4 MPa. Typically, C_f varied from 0.90–0.97, indicative of how slight variations in crucible-nozzle geometry affected the stream flow even when the same pressure was applied.

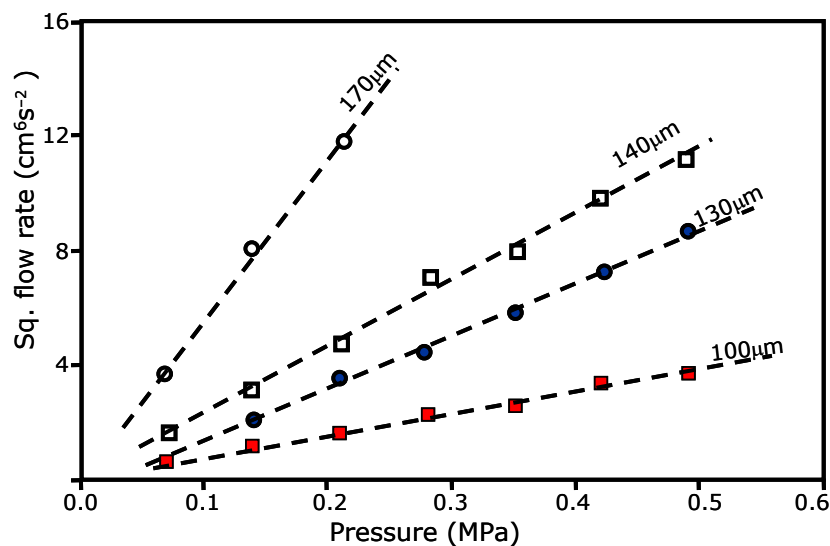


Figure 1. Flow curves showing relationships between square flow rate and applied pressure from water experiments for characterising flow coefficients.

3. Results and Discussion

3.1. Factors Affecting Stability of Melt Jet

In the rotating water bath process, it has long been recognised that the success of wire formation depends on (e.g., refs [6,7,35,36]):

- Nozzle clearance distance from cooling liquid
- Nozzle/melt jet diameter
- Ratio of melt jet velocity to that of the cooling liquid
- Melt super heat
- Alloy composition

All these are somehow related to the stability of the jet and are required to be optimised in order to cast wire continuously. The case of optimisation conditions in rotating water bath process is emphasised in the early reports for amorphous wire [6,13,35] and recently for crystalline Cu-Al-based alloys [38].

The casting conditions when using laser drilled multiple nozzles were summarised earlier [35]. These are concerned largely with stabilising the melt jets and maintaining their geometry in the transition from liquid melt to solid metallic glass wire. Here, each of these process parameters are considered as to how they affect the melt stream stability and how they determine the critical limits in the wire casting process.

3.2. Nozzle Clearance Distance

The distance between the nozzle tip and the water surface is important to wire formation. The optimum distance was found to be 2–4 mm. In the multi-stream configuration [35], it was important to use optically flat glass discs for drilling of orifices located in the nozzle base with the line of the orifice perpendicular to the direction of water flow, in order to maintain the same distance to the water surface by all of the melt streams. A slight curvature tended to develop on the flat disc as a result of fusion to the crucible base, but this generally had no perceptible effect on the ability to cast geometrically acceptable glassy wires. It was practically difficult to bring the nozzle tip closer than 2 mm to the surface of the water because of the risk of contact with the cooling water which results in cracking due to thermal shock. On the other hand, distances of greater than 4 mm usually led to stream break up and the formation of powder or short pieces of fibres.

It is important to consider the contribution of nozzle clearance distance to the stability of melt stream. Due to the effect of surface tension and viscosity, a liquid jet will tend to break into droplets. The theoretical and experimental studies of break up length of a free jet has attracted lots of attention [39,40] and the critical parameter to establish stability is conventionally expressed as the length to diameter ratio (L/d). The critical (L/d) ratio for a coherent isothermal liquid jet depends on the streaming conditions characterised by dimensionless numbers and can be expressed by the modified Weber equation [12,39]:

$$L/d = \left[\sqrt{We} + 3 \frac{We}{Re} \right] \ln \left(\frac{d}{2\epsilon_0} \right) \quad (2)$$

where We is the Weber number given by $We = \left(\frac{\rho v_m^2 d}{\sigma} \right)$ and Re is the Reynolds number given by

$Re = \frac{\rho v_m d}{\eta}$, σ , ρ , and η , are respectively the surface tension, density and dynamic viscosity of the melt.

The log term $\ln \left(\frac{d}{2\epsilon_0} \right)$ is an experimental parameter relating to the perturbation at the emergence of the jet from the nozzle and is approximately 12 for a wide variety of liquids and streaming conditions [38]. Typical wire casting conditions, for which $v_m \approx 10 \text{ ms}^{-1}$, and taking the values of melt physical properties given in [41], imply $We \approx 10$ and $Re \approx 10^4$, thus giving L/d ratio of approximately 40. A critical L/d of 40 is in accord with experimental observation and model prediction given in ref [40] for $Re = 10^3$ – 10^4 . For a 100 μm diameter melt jet, this corresponds to a jet break-up length of 4 mm. This is ostensibly in fairly good accord with the present experimentally observed critical nozzle distance of less than 4 mm for casting continuous metallic glass wire. However, it has been shown that the break-up length for an oxide-forming melt is at least one order of magnitude greater than that predicted from Equation (2). Figure 2 shows a photograph of melt streams maintained at the typical wire casting

condition, and observed unbroken for lengths well over 20 mm. It is seen that a coherent jet could still be maintained under casting conditions for lengths well above the critical value predicted from Equation (2). Nevertheless, the inability to produce continuous amorphous wire with clearance distances over 4 mm was an indication of instability of the flow setting-in irrespective of oxide protection. The fact that, even beyond this predicted limiting length of 4 mm, short brittle fibres could still be produced suggests that nozzle-water clearance distance in itself is not strictly a limiting factor on the stability of the stream up to the point of entry of the jet into the quenching water. However, the distance needs to be kept to less than 4 mm, partly to minimise velocity rise due to gravitational acceleration and also to minimise air cooling of the melt stream and, thus, maximising the quenching rate required for the vitrification of the melt. For longer nozzle-water clearance, the drop in temperature imposed from air-cooling would reduce the temperature differential between the melt stream and the quenching medium and may, thus, result in a cooling rate below the critical cooling rate for glassy wire production.

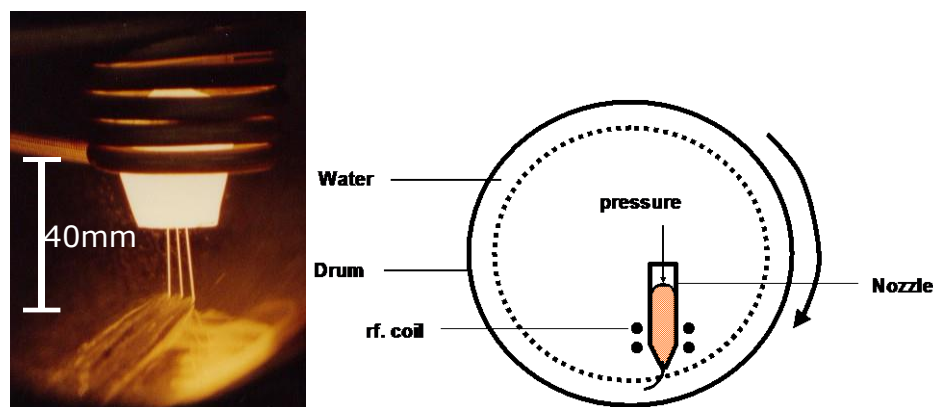


Figure 2. (a) Unbroken melt jet streams maintained for over 20 mm under streaming conditions. (b) Schematic diagram of the wire casting.

3.3. Nozzle Diameter and Jet Contraction

For most compositions investigated, continuous wire production was limited to diameters between 80 and 150 μm . Outside these ranges, powder or short pieces of fibres were produced, indicating an unstable melt stream during casting attempts. The lower limit of 80 μm was imposed by the shorter distance at which instability sets in and also by the difficulty of initiating flow of the viscous melt through the nozzle. In order to increase the L/d ratio (as predicted in Equation (2)), it would have been necessary to increase cast pressure which again was limited by the ability of the crucible material to withstand higher pressures at the casting temperatures. Additionally, at small diameters, blockage of nozzles was a problem that constantly disturbed and caused instability in the melt stream.

At larger nozzle diameters ($d > 150 \mu\text{m}$), the cooling rate becomes a problem. Although it was easier to maintain a stable stream (as predicted by Equation (2)), from heat transfer considerations, the average cooling rate of the melt was reduced for large diameters. This had implications for the solidification rate. The success of forming continuous wire is ultimately dependent on rapid solidification of the molten jet stream. The longer the solidification times, experienced with larger diameters, the greater the effect of forces related to momentum change as the melt stream changed course in the stream on confluence. Incomplete solidification would therefore cause the break-up of the stream leading to powders or short

fibres. Additionally, the reduced cooling rates may be below the critical rate for glass formation in that particular composition being cast, thus resulting in a partially or fully crystalline brittle wire.

Generally, it was observed that the wire diameter is about 10% smaller than the nozzle diameter, thus signifying a jet contraction in flight during casting. Such contraction can be explained if we consider the relaxation of the velocity profile that exists across the jet stream. A simplified approach to predicting such contraction from velocity relaxation would be to assume a fully developed laminar flow across the nozzle at the point of exit. The velocity profile as depicted in Figure 3 can then be expressed as that given for a laminar non-compressible fluid over a flow length L as [37]:

$$v = \frac{\Delta PR^2}{4\eta L} \left[1 - \left(\frac{r}{R} \right)^2 \right] \quad (3)$$

where R is the radius of the nozzle and r represents the radial distance from the centreline.

It could be shown that the mass flow rate (\dot{m}) is [37]:

$$\dot{m} = \int_{r=0}^{r=R} 2\pi r \rho \frac{\Delta PR^2}{4\eta L} \left[1 - \left(\frac{r}{R} \right)^2 \right] dr = \frac{\pi \rho \Delta PR^4}{8\eta L} \quad (4)$$

On emergence from the nozzle, the melt stream condition is equivalent to that in which the fixed boundary of the nozzle is suddenly removed. The streamlines near the boundary, having initially zero velocity, will accelerate. The most simplified scenario is to assume acceleration to the centre line velocity which is the maximum of the velocity profile equation (Equation (3)) and is given by [37]:

$$v_{\max} = \frac{\Delta PR^2}{4\eta L} \quad (5)$$

The mass flow rate \dot{m}' of a contracted free jet with reduced radius R' is given by:

$$\dot{m}' = \rho v_{\max} \times Area = \frac{\rho \Delta PR^2}{4\eta L} \times \pi (R')^2 \quad (6)$$

For mass conservation, we expect that flow rate remains the same before and after jet contraction and this implies that:

$$\frac{\rho \Delta PR^2}{4\eta L} \times \pi (R')^2 = \frac{\rho \Delta PR^4}{8\eta L} \quad \text{or} \quad R' = \frac{1}{\sqrt{2}} R \quad (7)$$

This analysis predicts a jet contraction of $1 - 1/\sqrt{2}$ (~30%) which clearly is an overestimation when compared with the experimental results of about 10%. A drawback to the theoretical prediction of jet contraction in short bore orifices as in nozzles for wire casting can be the incomplete description of hydrodynamic flow within the jet. A schematic model of flow development is shown in Figure 4. A semi-empirical fluid mechanics approach suggests [37] that, to fully establish (99%) laminar flow, an L/d ratio of 116 is required. This translates to bore lengths of greater than 12 mm for a typical nozzle orifice diameter of 100 μm , normally used for wire casting. In practice, nozzles are converging and with lengths of the order of a few millimeters. The assumption of a fully developed laminar flow in this analysis, therefore, cannot truly represent the streaming conditions of the nozzle in the wire casting

process. Nevertheless, the analysis here qualitatively explains the observed contraction from a possible relaxation of a streamline velocity profile across the jet in free flight.

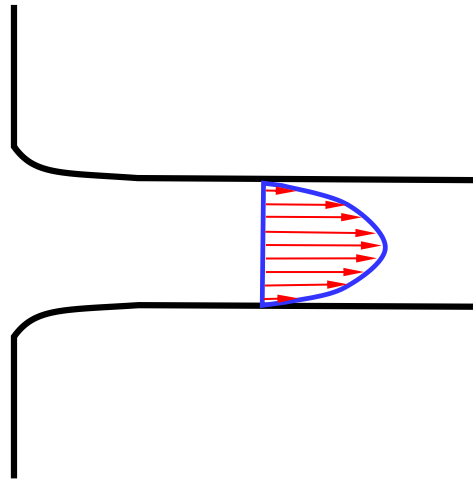


Figure 3. Schematic representation of velocity profile in a fully developed laminar flow.

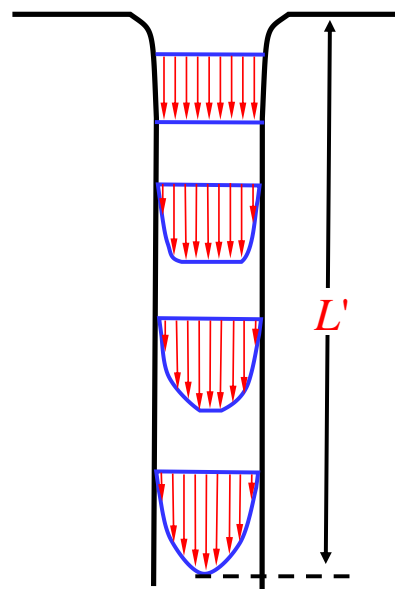


Figure 4. Schematic representation of flow development showing critical length for fully developed laminar flow.

3.4. Melt Superheat

The optimum superheat for continuous wire formation was found [35] to be 100–150 K. Lower superheats cause fluidity problems resulting in premature nozzle blockage that prevented the formation of a coherent jet. Excessive superheat could lead to nozzle distortion that affects the dynamics of fluid flow through the nozzle. Moreover, large superheats imply a longer solidification time which would be detrimental to maintaining a continuous flow of the melt stream before initial solidification occurs. It has been shown [35] that large superheat resulted in partially crystalline wire as indicated by the sharp crystalline peaks of XRD pattern for wire samples with superheat greater than 100 K. For an alloy composition of $\text{Fe}_{77.5}\text{Si}_{7.5}\text{B}_{15}$, the role of excessive superheat on melt in the cast wire is shown on the

DSC crystallisation thermograms in Figure 5. Here, it is seen that crystallisation peaks for metallic glass cast at high melt temperature (1450 °C) are much lower smaller compared to those cast at lower temperatures (*i.e.*, with less superheat). The indication then is that for excessive superheat, complete vitrification is not achieved. The longer cooling intervals associated with a large superheat resulted in incomplete vitrification, and it is particularly more evident for larger diameters, for which the margin for glass formation is narrower for most compositions.

Ordinarily, for heat transfer considerations, we would expect a large superheat to translate to a higher average cooling rate of the melt if complete Newtonian cooling was responsible for the heat transfer. However, limitations exist in heat transfer coefficients when a solid is being cooled in a liquid medium from a temperature well above the boiling point of the cooling liquid. In this case, expected boiling (at 100 °C) would mean the wire would be encased in a steam jacket initially and the increased temperature potential from additional superheat would not lead to increased average cooling rate as would be expected from a fully Newtonian cooling; rather, the longer solidification time would prove the kinetic lag for diffusive atomic rearrangement into crystalline structure. Although superheat is not critical to melt jet stability, its role in reducing glass-forming can lead to the formation of partially crystalline and subsequently brittle wire that tends to break into short fibres or fragment into powders.

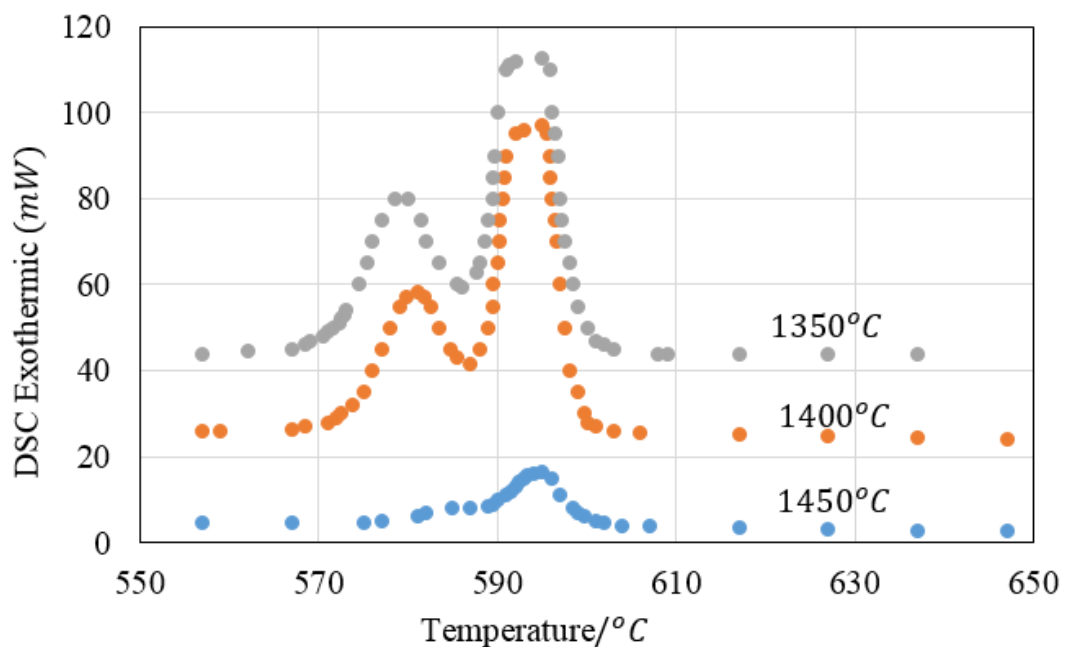


Figure 5. Effect excessive superheat on the degree of vitrification on as-cast wire.

3.5. Effect of Water and Jet Velocity

Velocity mismatch between melt stream and cooling stream has long been recognised [5] as one of the possible contributors to break up forces that cause instability in the melt stream. In the water bath process, the ratio of the velocities of the melt stream and the water bath (v_m/v_w) has been found to be a critical factor for continuous wire formation. Depending on alloy composition, we have found [35] that the critical values of v_m/v_w range from 1.1–1.21, still within the wider range of 1–2 proposed originally by Masumoto *et al.* [6]. However, these studies were directed at casting both crystalline and amorphous alloys wires. Some effects of the magnitude of v_m/v_w on the morphology of wire for the glass-forming

alloy FeCrSiB are shown in Figure 6. These illustrate the effects of the various deformation forces on the liquid jet prior to solidifying.

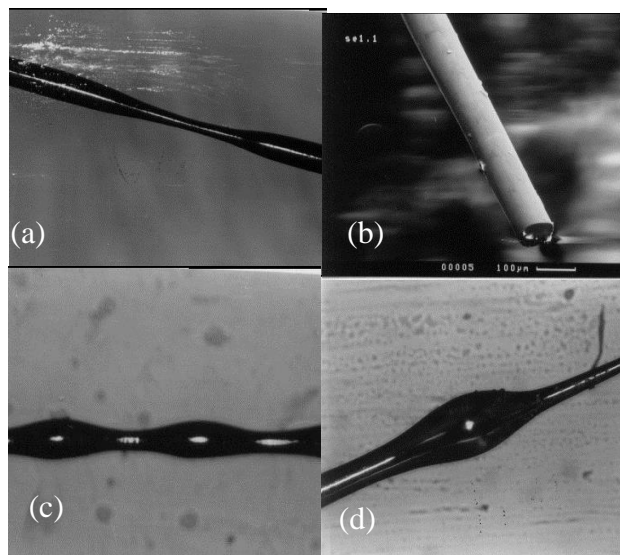


Figure 6. Some of the effects of v_m/v_w ratios on wire morphology (optical for (a) (c) and (d); and SEM for (b)) wire morphology (a) $v_m/v_w = 1.3$ (b) $v_m/v_w = 1.1$ (c) $v_m/v_w = 0.9$ (d) $v_m/v_w = 1.5$.

The significance of the velocity ratio v_m/v_w for this casting process lies in the forces imposed on the melt jet as it changes course from an initial stream velocity v_m to be in confluence with the quenching water bath having a velocity v_w . Previous studies suggest matching the two stream velocities would maintain continuity in the transition of the molten stream to solid filament. However, the change in direction of jet on entry into the water imposes a substantial force on it. The velocity change of the jet and the force exerted on it on entry into the water bath are depicted in Figure 7. Resolving the velocities, and applying Newton’s second law to the jet trajectory, the force \vec{F} imposed from the momentum change is given in vector form by the equation:

$$\vec{F} = \dot{m} \{ (v_w \sin \phi) i + (v_m - v_w \cos \phi) j \} \tag{8}$$

where i and j are unit vectors respectively along the horizontal and vertical axes.

The direction and magnitude of \vec{F} is most critical to the stability of the jet. The direction depicted by angle θ in Figure 7, is given by:

$$\theta = \tan^{-1} \left\{ \left(\frac{v_m}{v_w} - \cos \phi \right) \frac{1}{\sin \phi} \right\} \tag{9}$$

We can consider two limiting conditions for the stability of the jet; one for which magnitude of the force $|F|$ is minimum but completely shearing and the other where the direction indicates an equal distribution between the shear and tensile or compression; i.e. we choose $\theta = 45^\circ$. In the case of the former, $v_m/v_w = \cos \phi$. For the limiting condition of $\theta = 45^\circ$, $v_m/v_w = \cos \phi + \sin \phi$. In practice, wire casting successfully relies on minimising magnitude of the interaction force and optimising its

distribution into shearing and direct. It is therefore expected that an optimum casting condition would be between these two limiting conditions as:

$$\cos \phi < v_m/v_w < (\cos \phi + \sin \phi) \quad (10)$$

It is clear that stability of jet due to momentum change is dependent on both the velocity ratio v_m/v_w and the jet entrant angle ϕ . Since angle ϕ is normally kept constant, (though in our experiments it was kept at 30°) we can redefine the range for which the critical v_m/v_w value must lie in the range: $0.87 < v_m/v_w < 1.37$. This is consistent with experimental observations for which critical v_m/v_w for FeCrSiB melt was found to be 1.1–1.21. Outside the optimal range, the direction θ of the imposed force would upset the force component allowing either of the shearing or compressive forces to predominate leading respectively to powder or deformed wire. The criticality of the ratio v_m/v_w is confined to a narrow range so that it gives a minimum shear component of force imposed by the momentum change.

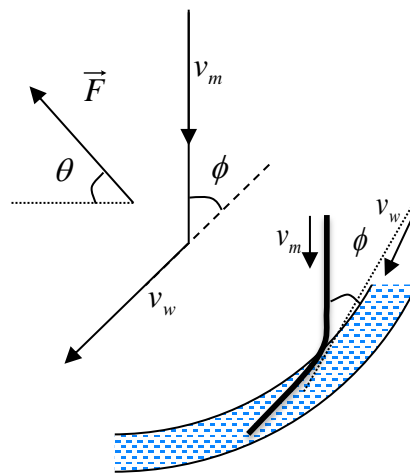


Figure 7. Velocity change and force exerted at the confluence of melt and water streams.

3.6. Effect of Alloy Composition

It was found [35] that for the compositional series $\text{Fe}_{85-x}\text{Si}_x\text{B}_{15}$, a minimum silicon content of 5% was required for continuous wire formation even with very strict process control. Replacement of Fe with Cr was also found to increase the wire forming ability, within a broader window of values of v_m/v_w for continuous wire formation.

The influence of oxide formers on wire forming ability has long been recognized [10]. The natural tendency of a melt stream to disintegrate into droplet decreases with the presence of a coherent oxide skin. It is consistent with the earlier analysis in that we expect a larger than predicted L/d ratio and thus a longer break-up length of free jet for a strong oxide-forming melts. The presence of an oxide skin on a melt would lead to greater shear resistance of the free jet. This would stabilize the jet against breakage notably when the momentum changed as the melt stream altered course as it travelled through confluence and finally achieved the speed of the quenching water.

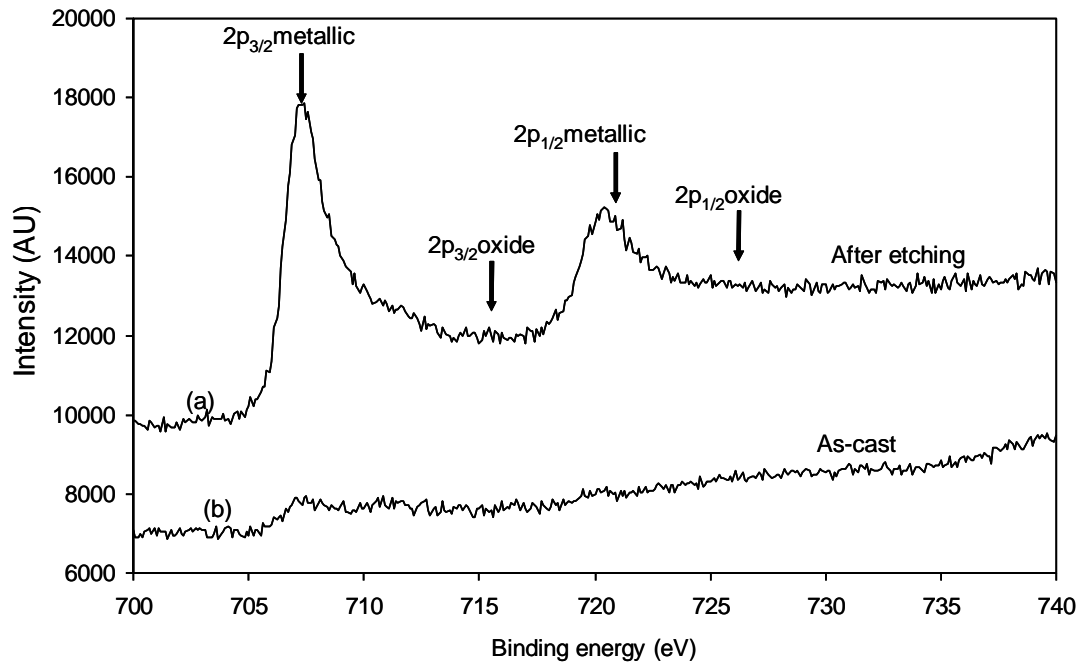


Figure 8. XPS Fe 2p in as-cast and after Ar^+ sputtering.

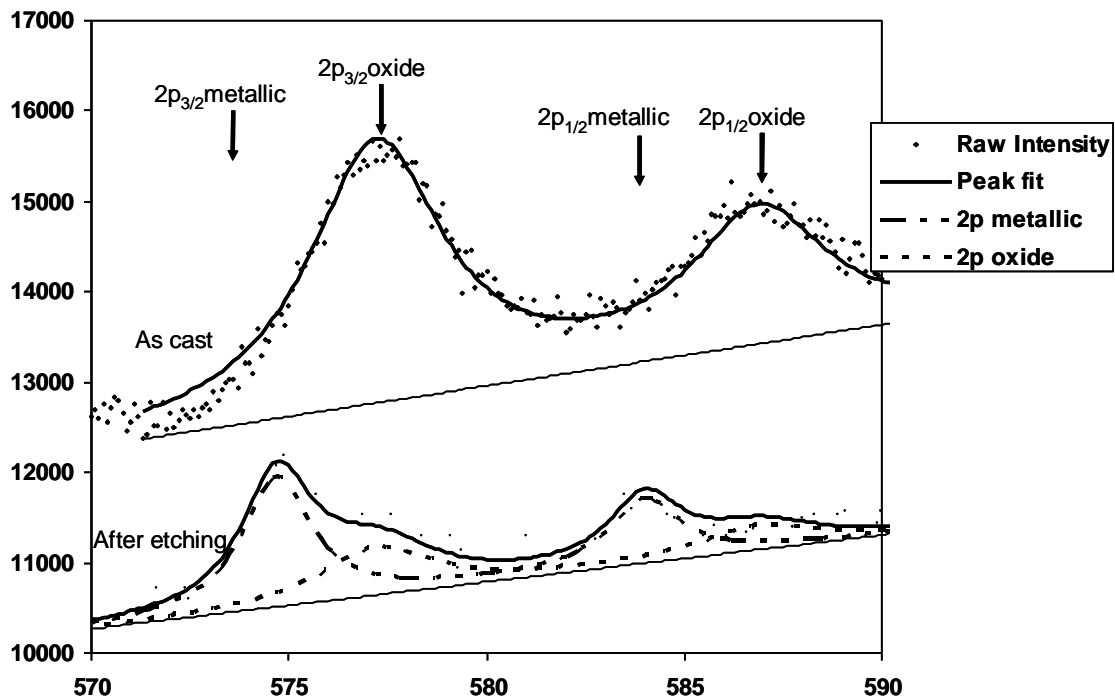


Figure 9. XPS Cr 2p peak fitting for standard Cr and Cr_2O_3 for as-cast wire and after ion sputtering.

The role of Si and Cr in forming oxides was confirmed through surface analysis of cast wires of composition $\text{Fe}_{69.5}\text{Cr}_8\text{Si}_{7.5}\text{B}_{15}$ with X-ray photo electron spectroscopy (XPS). Figure 8 shows the Fe 2p characteristic spectrum for as-cast and Ar^+ sputtered wire samples. It is clear that the surface has very weak Fe signal on the as-cast sample but the Fe 2p signal becomes more pronounced after prolonged etching that removed the surface oxide. The characteristic Fe $2p_{3/2}$ and $2p_{1/2}$ are clearly indicative of metallic, thus confirming that the surface composition is essentially different from the bulk. Similar

Cr-2p and Si-2p lines are respectively shown in Figures 9 and 10. It is shown in these figures that both the Cr 2p and Si 2p XPS characteristic peaks for the as-cast wire fit more closely with standard oxide spectra. These characteristic peaks move closer to metallic after Ar⁺ sputtering. The comparison of the XPS spectra (Figures 8–10) for as-cast and sputtered samples confirms the compositional difference of the surface and the core of the wire samples. The present XPS evidence suggests that the surface consisted essentially Si and Cr oxides. Semi-quantitative analyses of these peaks based on integrated areas and applying sensitivity factors, suggest that Cr/Fe and Si/Fe atomic ratios were respectively 1.2 and 3.9. These values are much higher than the nominal Cr/Fe and Si/Fe atomic ratios of ≈ 0.1 that are expected from the nominal composition of the bulk alloy.

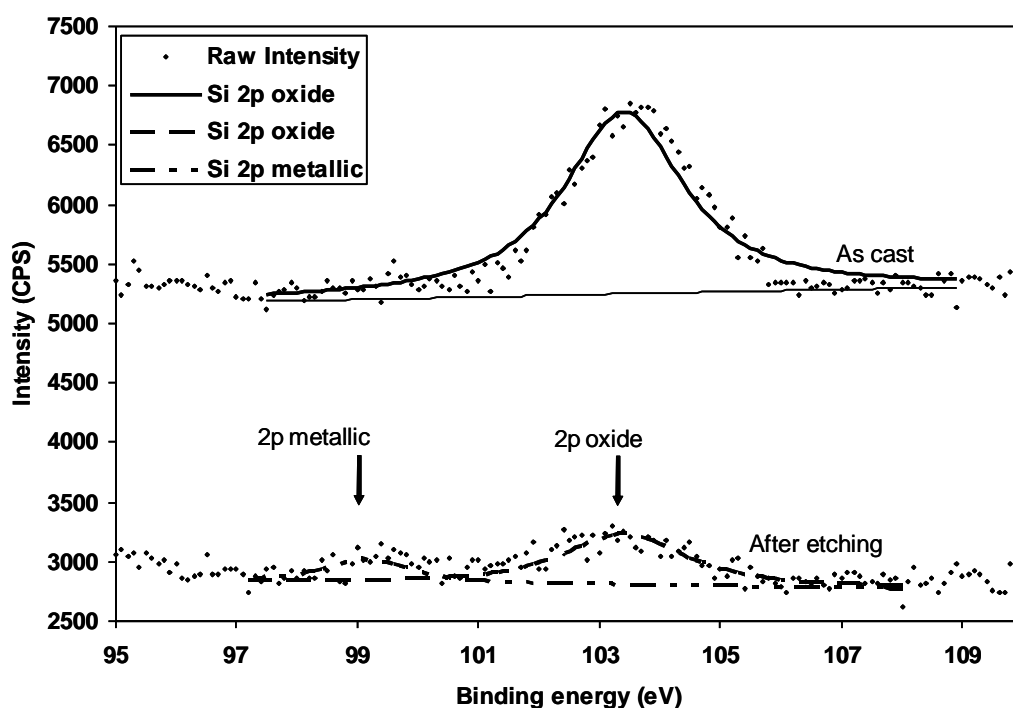


Figure 10. XPS Si 2p peak fitting for standard SiO₂ for as-cast wire and after ion sputtering.

It is somewhat surprising that the Fe 2p for the un-sputtered samples indicate almost no presence of Fe. The result of the Fe 2p due to light etching confirmed this is only limited to the surface and must be related to the oxide-forming tendencies of the constituents Si and Cr elements. The relative influence of elements on oxide formation according to thermodynamic drive [42] derived from free energies for oxide formation would be of the order Si > Cr > Fe and this is consistent with the present XPS observations. Since both Si and Cr at high temperatures have much higher negative free energies for oxide formation, even their presence in relatively small concentration (7–8 at%) would give a thermodynamic and kinetic preference for their oxide formation over the main (Fe) alloy constituent. This XPS evidence confirms the important roles of Si and Cr in forming a coherent oxide skin which stabilizes the free flight of the melt jet and, thus, allows more flexibility with the process variables in forming wires.

4. Conclusions

Successful wire formation by the rotating water bath melt spinning technique depends on maintaining good stability of the melt stream and on minimizing any disturbances of this stream as it freezes. The

criticality of some of the process variables is determined by the narrow process window required for stabilizing and minimizing the disturbances to the melt stream. While nozzle diameters and melt superheat within the limits applicable are not strictly jet stability criteria, they play a critical role in complete glass formation and, thus, continuity of the final wire product. The most essential criteria for melt jet stability is the velocity ratio of melt to cooling water v_m/v_w as it relates to the direction of the force imposed on the melt as it comes into confluence with the cooling stream of water. The role of the oxide-forming elements Si and Cr is crucial to provide a strong Si/Cr oxide skin on the stream surface which resists the shearing force imparted on the melt stream as it is subjected to acceleration/deceleration when it enters the water bath at an oblique angle.

Acknowledgments

The wire casting experiments reported in this work were done at the laboratories of The University of Sheffield, UK, under the supervision of H.A. Davies.

Author Contributions

A.O. carried out the wire casting experiments and prepared the original draft. N.Y.V processed the XPS data, carried out the thermal analysis and contributed to literature review that form the basis for this manuscript.

Conflicts of Interest

The authors declare no conflict of interest.

References

1. Small, E. Apparatus for Making Wire Solder. U.S. Patent 262625, 1882.
2. Otstot, R.S.; Motern, J.W. Method and Apparatus for Improved Extrusion of Essentially Inviscid Jets. U.S. Patent 3,645,657, 1972.
3. Privott, W.J.; Cunningham, R.E. Low Viscosity Melt Spinning Process. U.S. Patent 3,715,419, 1973.
4. Kavesh, S. Apparatus for liquid quenching of free jet spun metal. U.S. Patent 3,845,805, 1976.
5. Adler, R.P.I. Melt Spinning Process and Machine. U.S. Patent 4,020,891, 1977.
6. Masumoto, T.; Hagiwara, M. Process for the Production of Fine Amorphous Metallic Wires. U.S. Patent 4,495,691, 1985.
7. Masumoto, T.; Hamashima, T.; Hagiwara, M. Method of Manufacturing Thin Metal Wire. U.S. Patent 4,614,221, 1986.
8. Hagiwara, M.; Menjiu, A.; Kohachi, N.; Masaru, K.; Yoshianao, Y.; Miyuri, S. Fine Amorphous Metal Wire. U.S. Patent 4,806,179, 1989.
9. Larin, V.S.; Torcunov, A.V.; Zhukov, A.; Gonzalez, J.; Vazquez, M.; Panina, L. Preparation and properties of glass-coated microwires. *J. Magn. Magn. Mater.* **2002**, *249*, 39–45.
10. Inoue, A.; Krause, J.T.; Masumoto, T.; Hagiwara, M. Young's modulus of Fe-, Co-, Pd- and Pt-based amorphous wires produced by the in-rotating-water spinning method. *J. Mater. Sci.* **1983**, *18*, 2743–2751.

11. Shalyginaa, E.E.; Umnova, N.V.; Umnov, P.P.; Molokanov, V.V.; Samsonova, V.V.; Shalygin, A.N.; Rozhnovskaya, A.A. Specific Features of Magnetic Properties of “Thick” Microwires Produced by the Ulitovsky–Taylor Method. *Phys. Solid State* **2012**, *54*, 287–292.
12. Frommeyer, G.; Frech, W. Continuous casting and rapid solidification of wires produced by a newly developed shape flow casting technique. *Mater. Sci. Eng. A* **1997**, *226*, 1019–1024.
13. Sarkar, P.; Roy, R.K.; Panda, A.K.; Mitra, A. Optimization of process parameters for developing FeCoSiB amorphous microwires through in-rotating-water quenching technique. *Appl. Phys. A* **2013**, *111*, 575–580.
14. Vazquez, M. Soft magnetic wires. *Phys. B* **2001**, *299*, 302–313.
15. Gavrilyuk, A.V.; Gavrilyuk, A.A.; Kovaleva, N.P.; Mokhovikov, A.Y.; Semenov, A.L.; Gavrilyuk, B.V. Magnetic properties of Fe₇₅Si₁₀B₁₅ amorphous metallic wires. *Phys. Metals Metallogr.* **2006**, *101*, 434–439.
16. Sarkar, P.; Roy, R.K.; Mitra, A.; Panda, A.K.; Churyukanov, M.; Kaloshkin, S. Effect of Nb and Cr incorporation on the structural and magnetic properties of rapidly quenched FeCoSiB microwires. *J. Magn. Magn. Mater.* **2012**, *324*, 2543–2546.
17. Zhang, D.; Chen, K.; Jia, X.; Wang, D.; Wang, S.; Luo, Y.; Ge, S. Bending fatigue behaviour of bearing ropes working around pulleys of different materials. *Eng. Fail. Anal.* **2013**, *33*, 37–47.
18. Vazquez, M.; Marin, P.; Olofinjana, A.O.; Davies, H.A. The magnetic properties of FeSiBCuNb wires during the first stages to the nanocrystallization process. *Mater. Sci. Forum* **1995**, *179–181*, 521–526.
19. Vazquez, M. Giant magneto-impedance in soft magnetic “wires”. *J. Magn. Magn. Mater.* **2001**, *226*, 693–699.
20. Mokhiev, I.I.; Chueva, T.R.; Zabolotnyi, V.T.; Umnov, P.P.; Umnova, N.V.; Molokanov, V.V. Strength and Plastic Properties of Amorphous Cobalt Alloy Wires Produced by Various Melt Quenching Methods. *Russ. Metall. (Metally)* **2010**, *2011*, 345–349.
21. Luo, Y.; Peng, H.X.; Qin, F.X.; Ipatov, M.; Zhukova, V.; Zhukov, A.; Gonzalez, J. Fe-based ferromagnetic microwires enabled meta-composites. *Appl. Phys. Lett.* **2013**, *103*, 251092.
22. Qin, F.; Peng, H.-X. Ferromagnetic microwires enabled multifunctional composite materials. *Prog. Mater. Sci.* **2013**, *58*, 183–259.
23. Zhao, Y.Y.; Li, H.; Hao, H.Y.; Li, M.; Zhang, Y.; Liaw, P.K. Microwires fabricated by glass-coated melt spinning. *Rev. Sci. Instrum.* **2013**, *84*, 075102.
24. Zhukov, A.; Chichay, K.; Talaat, A.; Rodionova, V.; Blanco, J.M.; Ipatov, M.; Zhukova, V. Manipulation of magnetic properties of glass-coated microwires by annealing. *J. Magn. Magn. Mater.* **2015**, *383*, 232–236.
25. Varga, R.; Ryba, T.; Vargova, Z.; Saksl, K.; Zhukova, V.; Zhukov, A. Magnetic and structural properties of Ni-Mn-Ga Heusler-type microwires. *Scr. Mater.* **2011**, *65*, 703–706.
26. Zhukov, A.; Rodionova, V.; Ilyn, M.; Aliev, A.M.; Varga, R.; Michalik, S.; Aronin, A.; Abrosimova, G.; Kiselev, A.; Ipatov, M.; Zhukova, V. Magnetic properties and magnetocaloric effect in Heusler-type glass-coated NiMnGa microwires. *J. Alloys Compd.* **2013**, *575*, 73–79.
27. Zhukova, V.; Aliev, A.M.; Varga, R.; Aronin, A.; Abrosimova, G.; Kiselev, A.; Zhukov, A. Magnetic Properties and MCE in Heusler-Type Glass-Coated Microwires. *J. Supercond. Novel Magn.* **2013**, *26*, 1415–1419.

28. Zhukova, V.; Ipatov, M.; Granovsky, A.; Zhukov, A. Magnetic properties of Ni-Mn-In-Co Heusler-type glass-coated microwires. *J. Appl. Phys.* **2014**, *115*, 17A939.
29. Zhukova, V.; Rodionova, V.; Fetisov, L.; Grunin, A.; Goikhman, A.; Torcunov, A.; Aronin, A.; Abrosimova, G.; Kiselev, A.; Perov, N.; *et al.* Magnetic Properties of Heusler-Type Microwires and Thin Films. *IEEE Trans. Magn.* **2014**, *50*, doi:10.1109/TMAG.2014.2324494.
30. Zhukov, A.; Gonzalez, J.; Blanco, J.M.; Vazquez, M.; Larin, V. Microwires coated by glass: A new family of soft and hard magnetic materials. *J. Mater. Res.* **2000**, *15*, 2107–2113.
31. Chizhik, A.; Zhukov, A.; Gonzalez, J. Magnetic properties of sub-micrometric Fe-rich wires. *Thin Solid Films* **2013**, *543*, 130–132.
32. Varga, R.; Zhukov, A.; Ipatov, M.; Blanco, J.M.; Gonzalez, J.; Zhukova, V.; Vojtanik, P. The influence of glass coating on the single domain wall potential in amorphous glass-coated Fe-based microwires. *J. Magn. Magn. Mater.* **2006**, *304*, E519–E521.
33. Qin, F.; Peng, H.X.; Tang, J.; Qin, L.C. Ferromagnetic microwires enabled polymer composites for sensing applications. *Composites Part A* **2010**, *41*, 1823–1828.
34. Zhukova, V.; Cobeno, A.F.; Zhukov, A.; Blanco, J.M.; Puerta, S.; Gonzalez, J.; Vazquez, M. Tailoring of magnetic properties of glass-coated microwires by current annealing. *J. Non-Cryst. Solids* **2001**, *287*, 31–36.
35. Olofinjana, A.O.; Kern, J.H.; Daves, H.A. Effects of process variables on the multi-strand casting of high strength sub-millimetre metallic glass wire. *J. Mater. Process. Technol.* **2004**, *155*, 1344–1349.
36. Olofinjana, A.O.; Kern, J.H.; Davies, H.A. Multistrand casting of amorphous alloy wire. *Mater. Lett.* **1995**, *23*, 55–57.
37. Finnmore, E.; Franzini, J. *Fluid Mechanics with Engineering Applications*; McGraw-Hill Education: New York, NY, USA, 2001.
38. Zeller, S.; Gnauk, J. Shape memory behaviour of Cu-Al wires produced by horizontal in-rotating-liquid-spinning. *Mater. Sci. Eng. A* **2008**, *481*, 562–566.
39. Castrejon-Pita, A.A.; Castrejon-Pita, J.R.; Hutchings, I.M. Breakup of Liquid Filaments. *Phys. Rev. Lett.* **2012**, *108*, 074506.
40. Richards, J.R.; Lenhoff, A.M.; Beris, A.N. Dynamic breakup of liquid jets. *Phys. Fluids* **1994**, *6*, 2640–2655.
41. Liu, J.; Arnberg, N.; Backstrom, S.; Savage, S. Fundamental Parameters in the direct wire casting process. *Mater. Sci. Eng. A* **1988**, *98*, 21–24.
42. Darken, L.S. *Physical Chemistry of Metals*; McGraw-Hill: New York, NY, USA, 1953.